analytical chemistry

Article

Cite This: *Anal. Chem.* 2018, 90, 8831−8837

pubs.acs.org/ac

Multisensor Imaging—From Sample Preparation to Integrated Multimodal Interpretation of LA-ICPMS and MALDI MS Imaging Data

Matthias Holzlechner, Maximilian Bonta, Hans Lohninger, Andreas Limbeck, and Martina Marchetti-Deschmann*

Institute of Chemical Technologies and Analytics, TU Wien, Getreidemarkt 9, 1060 Vienna, Austria

Supporting Information

ABSTRACT: Laterally resolved chemical analysis (chemical imaging) has increasingly attracted attention in the Life Sciences during the past years. While some developments have provided improvements in lateral resolution and speed of analysis, there is a trend toward the combination of two or more analysis techniques, so-called multisensor imaging, for providing deeper information into the biochemical processes within one sample. In this work, a human malignant pleural mesothelioma sample from a patient treated with cisplatin as a cytostatic agent has been analyzed using laser ablation inductively coupled plasma mass spectrometry (LA-ICPMS) and matrix-assisted laser desorption/ionization mass spectrometry (MALDI MS). While LA-ICPMS was able to provide quantitative information on the platinum distribution along with the distribution of other elemental analytes in the tissue sample, MALDI MS could reveal full information on lipid distributions, as both modes of polarity, negative and positive, were used for measurements. Tandem MS experiments verified the occurrence of distinct lipid classes. All imaging analyses were performed using a lateral resolution of 40 μm, providing information with excellent depth of details. By analyzing the very same tissue section, it was possible to perfectly correlate the obtained analyte distribution information in an evaluation approach comprising LA-ICPMS and MALDI MS data. Correlations between platinum, phosphorus, and lipid distributions were found by the use of advanced statistics. The present proof-of-principle study demonstrates the benefit of data combination for outcomes beyond one method imaging modality and highlights the value of advanced chemical imaging in the Life Sciences.

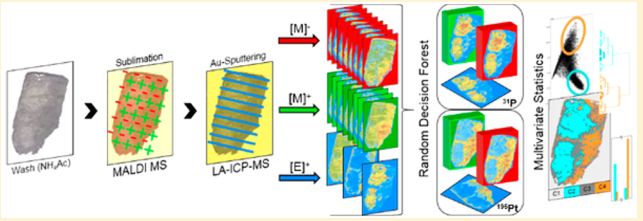

Modern clinical studies often rely on chemical analysis for in-depth investigation. Abundances of proteins, lipids, metabolites, or trace elements may, for example, be excellent indicators for the success of a therapy. Besides the knowledge of average analyte contents in tissue, gaining insight into the lateral distribution within a sample has attracted increased interest during the past years. Using solid sampling techniques, it is possible to analyze tissue sections generally with only minor sample preparation while maintaining the spatial integrity of the analytes of interest. Subsequently, obtained lateral distribution information can be compared with results from classical histological or immunohistochemical staining techniques.

The combination of different modalities offers a comprehensive analytical tool to answer biological questions that could otherwise not be answered. In the field of laterally resolved chemical analysis, there is a trend toward the combination of two or more technologies to provide more information than offered by a single modality.

While mass spectrometric imaging (MSI) offers high chemical specificity for visualizing and identifying distributions of several molecular species, it lacks the molecular depth that other methods provide and, thus, is typically combined with modalities that complement these features. MSI was and still is often combined with optical microscopy,[1] fluorescence microscopy,[2] near-field infrared microscopy,[3] electron microscopy,[4] coherent anti-Stokes Raman spectroscopy,[5] or Fourier transform infrared (FTIR) spectroscopy[6] to provide high-resolution morphological and structural information.

Because of the variety of ionization modalities, MSI can be multiplexed with itself to analyze different groups of compounds. In particular, matrix-assisted laser desorption/ionization mass spectrometry (MALDI MS) can be combined with a range of ionization mechanisms such as secondary ionization mass spectrometry (SIMS),[7,8] desorption electrospray ionization mass spectrometry (DESI MS),[9] or laser ablation inductively coupled plasma mass spectrometry (LA-ICPMS),[10] providing a more comprehensive analysis of the sample.

MALDI MS is a potent analytical technique for investigating larger intact molecules, such as proteins, peptides, lipids, and metabolites, features which are especially appealing for biological samples.[11,12] As being a solid sampling technique, the direct analysis of, for example, tissue samples is feasible, providing lateral distribution information on analytes. Thereby, matrix application to enable the analyte desorption and

Received: February 19, 2018
Accepted: June 30, 2018
Published: June 30, 2018

DOI: 10.1021/acs.analchem.8b00816
Anal. Chem. 2018, 90, 8831−8837

ionization process is a crucial step. If lateral resolution information is desired, special care has to be taken so as not to corrupt the natural analyte distribution in the sample. In the past years, methods such as matrix sublimation have been developed for this purpose.[13−15]

LA-ICPMS is a widely accepted method for elemental analysis of solid samples.[16,17] Due to its exceptional limits of detection (below the $\mu g\ g^{-1}$ range for most elements), achievable lateral resolutions down to the single-digit μm scale, and a quite extensive range of available possibilities for quantification, this technique has found its way into many disciplines of science.[18−20] Among them, Life Sciences have become a wide application range, with LA-ICPMS offering the possibility of depicting lateral distribution of trace elements in various types of biological samples.[21−23]

Since LA-ICPMS and MALDI MS offer complementary analyte information, excellent insight into the chemical nature of a sample can be gained by combination of these two techniques in a multisensor (different MS instrumentation), multimodal (different ionization modes) imaging (MSMMI) approach. Of course, using consecutive tissue thin-cuts might seem the most straightforward for this purpose, especially when the methods' requirements for sample preparation are different. However, even two consecutive tissue sections, cut at only some tens of μm distance, can show variation in analyte distributions. These may originate from the sample itself (cell size and shape) or from the sample preparation process (cutting accuracy). Therefore, analyzing the same sample using two different methods would be highly desirable to exclude the possibility of intersample variations but also to guarantee appropriate data quality for MSMMI approaches.

Multisensor imaging combining LA-ICPMS and MALDI MS on a single tissue sample has already been demonstrated in the literature[24,25] and has been applied to analyze patient samples treated with cisplatin or oxaliplatin.[10]

Some issues being crucial for analytic success are also outlined in these publications like sample preparation. MALDI MSI requires matrix application which can delocalize elements targeted by LA-ICPMS. However, performing LA-ICPMS before MALDI MSI is not possible because the sample is usually completely consumed.

Until today, no publication is available providing information on an integrated data evaluation strategy taking every gathered piece of information into account. Measuring in multiple modes from one tissue section is recognized by the community to be important for better comparison of MALDI images[26] and to gather information on analytes better detected in positive or negative ion mode,[27,28] but to our knowledge, the performance of three experiments from one tissue section has not been reported so far. We present data from different instruments (LA-ICPMS and MALDI MS), different types of analytes (elements and molecules), and different modes of ionization (ICP, MALDI in negative and positive ion mode), all measured from the same tissue section, and combine this information for a more comprehensive analysis based on supervised clustering. By using this statistical approach, a specified set of classes should be known in advance to classify a new data set into one of those classes. In the field of supervised classification, machine learning is getting more and more present in making predictions for new data sets. Data are analyzed using algorithms that look for correlated structures in the data that also correlate with a target outcome. Models used for classification include supervised neuronal networks, support vector machines, genetic algorithms, and random decision forests (RDFs).[29]

Therefore, the main goal of the study is to present a universal MSMMI approach for LA-ICPMS and MALDI MS imaging from one single tissue section. A human malignant pleural mesothelioma (MPM) sample from an individual being treated with cisplatin as a cytostatic drug has been used. The sample preparation strategy has been adjusted to fit the needs of each imaging method, LA-ICPMS and MALDI MSI, while providing the possibility of species identification by MALDI MS and quantification of elements, especially platinum, by LA-ICPMS. Ultimately, an integrated data evaluation strategy has been developed combining LA-ICPMS and negative and positive ion mode MALDI MS data. Advanced statistical analysis finally allowed the correlation of platinum distribution with certain lipids.

The results of the study prove the surplus of combining multiple instruments and measurement modes and underpin the importance of an integrated data analysis approach for valid findings.

MATERIALS AND METHODS

Materials. All reagents were purchased from Sigma-Aldrich (St. Louis, MO) with a purity of at least 99%, if not otherwise stated. Sections of a human MPM tissue were provided by the Department of Surgery and Comprehensive Cancer Center (Medical University of Vienna, AT). The tissue sections were sliced at a 10 μm thickness using a CM3050 cryostat from Leica Microsystems GmbH (Wetzlar, DE) and stored at −70 °C until further analysis. Ultrahigh quality water (ddH_2O) with a resistivity of <18.2 MΩ × cm @ 25 °C was obtained from a Simplicity system (Millipore, Billerica, MA). Conductive indium tin oxide (ITO) coated microscope glass slides were purchased from Delta Technologies (Loveland, MN). Ar used as collision gas in MALDI tandem MS (MS/MS) experiments as well as He and Ar used for LA-ICPMS measurements were purchased from Messer Austria GmbH (Gumpoldskirchen, AT) and were of grade 5.0 purity.

Tissue Preparation. Prior to MALDI mass spectrometry-based imaging (MSI), the frozen tissue sections were allowed to equilibrate to room temperature in a desiccator for ≥2 h and subsequently washed by submerging the slides in 50 mM ammonium acetate (pH 6.7, 4 °C, 4 times, 5 s each) to increase the negative ionization yield of lipids.[30] After each incubation step, the tissue was dried in a gentle stream of N_2 and finally stored in a desiccator for a minimum of 15 min before analyses.

Matrix Application for MALDI MS. Matrix deposition was performed using a home-built sublimation apparatus.[31] In a vacuum-sealed and pressure-controlled deposition chamber, 25.5 mg of 1,5-diaminonapthalene (1,5-DAN) was quantitatively vaporized and sublimed onto the tissue sections at 145 °C and 4.7 Pa, forming a homogeneous layer (0.23 mg cm^{-2}) of crystals. 1,5-DAN was the MALDI matrix of choice providing (1) rich lipid patterns in both negative and positive ion mode and (2) high vacuum stability[28] mandatory for multiple measurements of a single tissue sample.

Molecular Imaging by MALDI MS. MSI data were acquired on a MALDI TOF/RTOF mass spectrometer (ultrafleXtreme) using reflectron geometry and flexControl software v3.4 (Bruker Daltonics, Bremen, DE). The attenuator offset of the laser (smartbeam-II, wavelength 355 nm) was adjusted to 65%, and the laser fluence was set to 45%. The

DOI: 10.1021/acs.analchem.8b00816
Anal. Chem. 2018, 90, 8831−8837

mass range between 440 and 1700 Da was selected with ion suppression for analytes smaller than 340 Da. Imaging data was collected by analyzing at 40 μm lateral resolution in the negative mode, followed by the positive ion mode after offsetting x and y positions by 20 μm.[28] By using a laser repetition rate of 1 kHz, 100 shots per array position were summed up (no intraspot rastering). Mass spectra were calibrated externally using the cubic enhanced algorithm on singly charged ions of 1,5-DAN, bovine cardiolipin disodium salt, and castor oil. Data acquisition and image representation were carried out using flexImaging software v3.0 (Bruker Daltonics) and ImageLab software (Epina GmbH, Pressbaum, Austria). Acquired imaging data were normalized to the total ion current (TIC). MS/MS experiments in LIFT mode were performed for selected mass values for analyte identification, which was based on fragment information and comparison of parent ion information with theoretical m/z values according to the LIPID MAPS Structure Database (The LIPID MAPS Lipidomics Gateway, http://www.lipidmaps.org/) and the Metabolomics Workbench Metabolite Database (http://www.metabolomicsworkbench.org/), both University of California (San Diego, CA).

Elemental Imaging by LA-ICPMS. ICPMS data were obtained using a NWR213 laser ablation system (ESI, Fremont, CA) equipped with a frequency quintupled Nd:YAG laser (213 nm) in connection with a Thermo iCAP Qc (ThermoFisher Scientific, Bremen, DE). Experimental parameters were optimized in preliminary experiments to obtain the best possible trade-off between low analysis time and high data quality. All imaging analyses were performed using consecutive line scans at 40 μm laser beam diameter, 120 μm s^{-1} stage scan speed, 7.56 J cm^{-2} laser fluence, and 20 Hz repetition rate. Helium gas at a flow rate of 1 L min^{-1} was used as carrier gas. Using the ICPMS, signals of ^{31}P, ^{34}S, and ^{195}Pt were monitored at a quadrupole dwell time of 10 ms per isotope and a mass resolution of 300 $m/\Delta m$.

Prior to LA-ICPMS analysis, samples were coated with a thin layer of gold using a sputter coater (Agar B7340, Agar Scientific Ltd., Essex, U.K.). The gold layer is ablated simultaneously with the sample and serves as a pseudointernal standard. Such use has been reported earlier elsewhere.[32] The pseudointernal standard can be employed to mitigate matrix effects and allows the quantification of platinum after external calibration using printed patterns on paper.[33]

The combined workflow of the MSMMI experiment is shown in Figure 1.

Data Fusion, Spectral Descriptors, and Multivariate Analysis. MALDI MS and LA-ICPMS imaging data sets were combined into a MSMMI data set using the software package ImageLab (Epina GmbH, Retz, Austria) as previously described.[34] The multivariate analysis of the hyperspectral datacube is based on spectral descriptors (SPDCs), as earlier introduced in the context of mass spectrometry.[35] Thereby, each SPDC corresponds to a feature in the obtained mass spectra. For the MALDI MS data cubes with negative and positive polarities, SPDCs were created algorithmically using the Spectral Descriptor Generator (peak area width: 1 Da). SPDCs for the individual elements from the LA-ICPMS data cube were simply defined by applying single intensity descriptors of the signals.

Random decision forest (RDF)-based classifiers[36] are often used models for classification. Besides SPDCs, a set of training data must be defined to create a classifier based on RDF. Therefore, 20 individual image pixels were selected and assigned to the elemental distributions of both ^{31}P and ^{195}Pt within tissue using the data set editor. The set of SPDCs along with the training data were loaded in the Decision Forest Training Engine for classification (R, 0.5; no. of trees, 75).

SPDC-based principal component analysis (PCA), hierarchical cluster analysis (HCA), and k-means cluster analysis were applied to verify the RDF-based results. Further details on the definition of SPDCs, standardization and application of multivariate statistics to the MSMMI data sets, as well as introductions to the different statistical methods can be found elsewhere.[35,37]

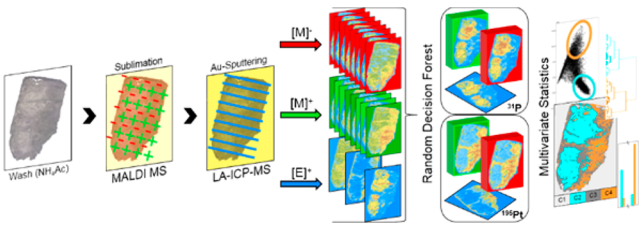

Figure 1. MSMMI workflow.

RESULTS AND DISCUSSION

Evaluation of Sample Carriers for Measurements. For MSI, tissue thin-cuts are usually mounted on sample carriers, providing conductive surfaces essential for sufficient analyte ionization. Thus, in the present case, ITO-coated glass slides were sought to be employed having the desired surface resistivity obligatory for MALDI. However, due to the high sensitivity of LA-ICPMS, background signals originating from these specific glass slides for the analytes of interest (i.e., phosphorus and platinum) had to be investigated to ensure suitability for elemental analysis. In contrast, usually employed sample carriers for LA-ICPMS are ordinary microscope glass slides or high-purity silicon wafers, which do not have the desired electric conductivity or transparency. Additionally, the absence of elements of interest in the MALDI matrix (usually polar substances with conjugated π systems required for effective UV light absorption) had to be proven to avoid contamination of the sample from this route.

For the purpose of this study, a blank ITO-coated glass slide underwent the matrix sublimation protocol described in the Materials and Methods. Single line scans with the same experimental conditions as those used for the following LA-ICPMS imaging experiments were applied, and the resulting analyte signals for ^{31}P, ^{34}S, and ^{195}Pt were collected. None of the isotopes showed signals which were significantly different for the gas blank of the respective measurement series (data not shown). Therefore, it could be concluded that neither ITO-coated target surfaces nor 1,5-DAN as the MALDI matrix of choice influence the analyte signals detected during LA-ICP MS imaging.

Elemental Bioimaging. Platinum is the active moiety of the administered drug cisplatin, and thus, its distribution within the malignant pleural mesothelioma (MPM) samples needed to be determined to obtain insights into the uptake mechanism of the drug. Applying a lateral resolution of 40 μm provided a good trade-off between minimal measurement time and good information content for medical interpretation. Only three elements of interest were investigated using this technique, namely, sulfur (^{34}S), phosphorus (^{31}P), and

DOI: 10.1021/acs.analchem.8b00816
Anal. Chem. 2018, 90, 8831−8837

platinum (^{195}Pt). While platinum served as the drug marker, sulfur and phosphorus were used as indicators for the presence of biological material. Derived elemental distribution images are shown in Figure 2.

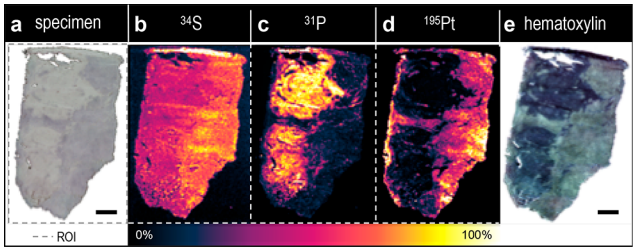

Figure 2. Microscopic image of the investigated sample (a), elemental distributions of sulfur (b), phosphorus (c), and platinum (d) and a consecutive tissue section of the same tumor after hematoxylin staining (e). The scale bar is 1 mm.

For the sake of simplicity of the illustration, only qualitative elemental distribution images are shown in the figures; quantification of the respective elements would not essentially influence the visual appearance of the distribution images. In the color scale used, black represents the lowest relative values, while yellow/white represents the highest relative values. In between, the colors blue (medium-low), red/purple (medium), and orange (medium-high) along with linear mixtures of these colors are used.

While the distribution of sulfur (Figure 2b) is rather homogeneous, phosphorus (Figure 2c) and platinum (Figure 2d) show distinct distribution patterns indicating different histological substructures of the tissue sample. This assumption is confirmed when comparing the elemental distributions with the hematoxylin stain of a consecutive thin-cut (Figure 2e).

Blue areas indicate viable tumor areas within the tissue, while unstained regions assumingly correspond to already recovered tissue. Distributions of phosphorus and platinum correlate well with this staining, where phosphorus is enriched in the viable tumor areas and platinum shows higher concentrations in the remaining areas of the sample. While the origin of the platinum signals is clear, no further information on the nature of phosphorus can be obtained using elemental bioimaging. Thus, molecular bioimaging capable of detecting larger intact molecules was required to answer this open question.

Molecular Bioimaging. Phospholipids are preferentially detected as either positive or negative ions depending on the headgroup of the different classes. Phosphatidylcholine (PC) and sphingomyelin (SM) lipids contain positively charged headgroups, whereas phosphatidylethanolamine (PE) and phosphatidylinositol (PI) are present in permanently neutral or negative charge states. Thus, for comprehensive analyses, MALDI MSI studies have to be performed in both negative- and positive-ion mode to gain maximum information depth of phospholipid distributions within a single tissue section. For accurate analyte correlation, ablation from the same tissue section is highly favorable; therefore, the tissue section was ablated by LA-ICPMS after MALDI MS analyses. The overall workflow is depicted in Figure 1, and examples of acquired analyte ion distributions are shown in Figure 3.

As two different samples have been used for obtaining the elemental distribution images shown in Figures 2 and 3, the respective distribution images differ slightly. Even though thin-

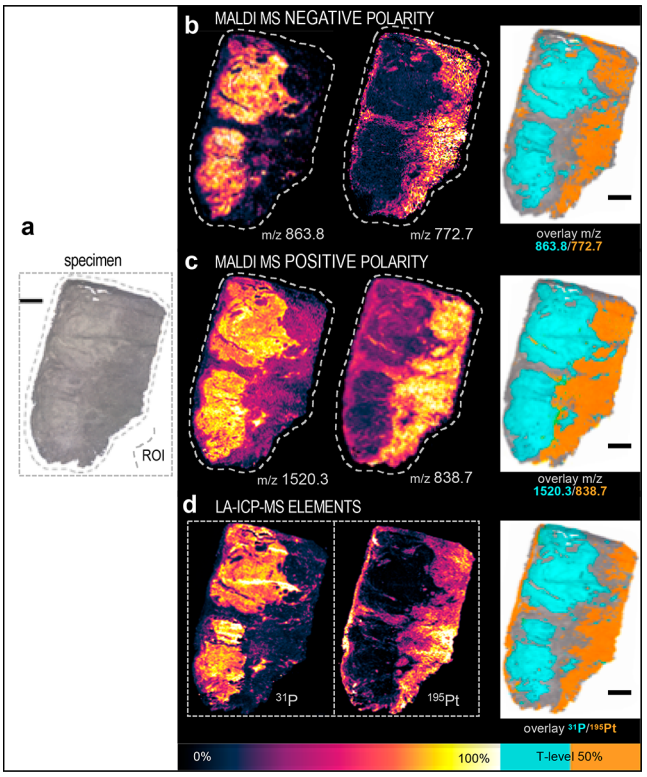

Figure 3. Microscopic image of a consecutive thin-cut showing rectangular and polygonal regions of interest (ROI) for LA-ICPMS and MALDI MS imaging experiments, respectively (a), negative ion intensity distributions of m/z 772.7 and 863.8 (b), positively charged ions of m/z 838.7 and 1520.3 (c), as well as elemental distributions of phosphorus and platinum (d), with all data collected from one tissue sample. Overlays of ion distributions are represented at an intensity threshold level of 50%. The scale bar is 1 mm.

cuts from the very same tumor sample have been used, variations may occur due to the cryo-cutting process, which lead to negligible differences even between two consecutive samples.

Interestingly, many of the detected molecular ions quite well resemble phosphorus and platinum distributions already revealed by LA-ICPMS imaging and hematoxylin staining. This holds true for both negative and positive MALDI MSI (see Supporting Information Figures S1 and S2 for profile spectra). Especially masses acquired with negative polarity correlate well with distributions of phosphorus and platinum. Contrarily, in the positive ion mode, ion distributions correlating with the elemental distribution of phosphorus are exclusively found in the higher mass range (1400−1650 Da). Due to the nature of their ionization, it can be certainly assumed that these m/z values represent phospholipid dimers which are usually formed at higher concentrations of the species in the sample during the MALDI process. Also, the corresponding monomers can be identified in the respective mass spectra.

MALDI Tandem MS (MS/MS) Analysis. Analyte identification in the viable tumor area is of special interest to confirm the supposed presence of phospholipids. One of the most critical issues in MALDI TOF-based MSI is the fact that analyte concentrations per pixel are extremely low, usually resulting in fragment ion spectra of poor quality (S/N, mass accuracy). In addition, not only the most abundant analyte is

DOI: 10.1021/acs.analchem.8b00816
Anal. Chem. 2018, 90, 8831−8837

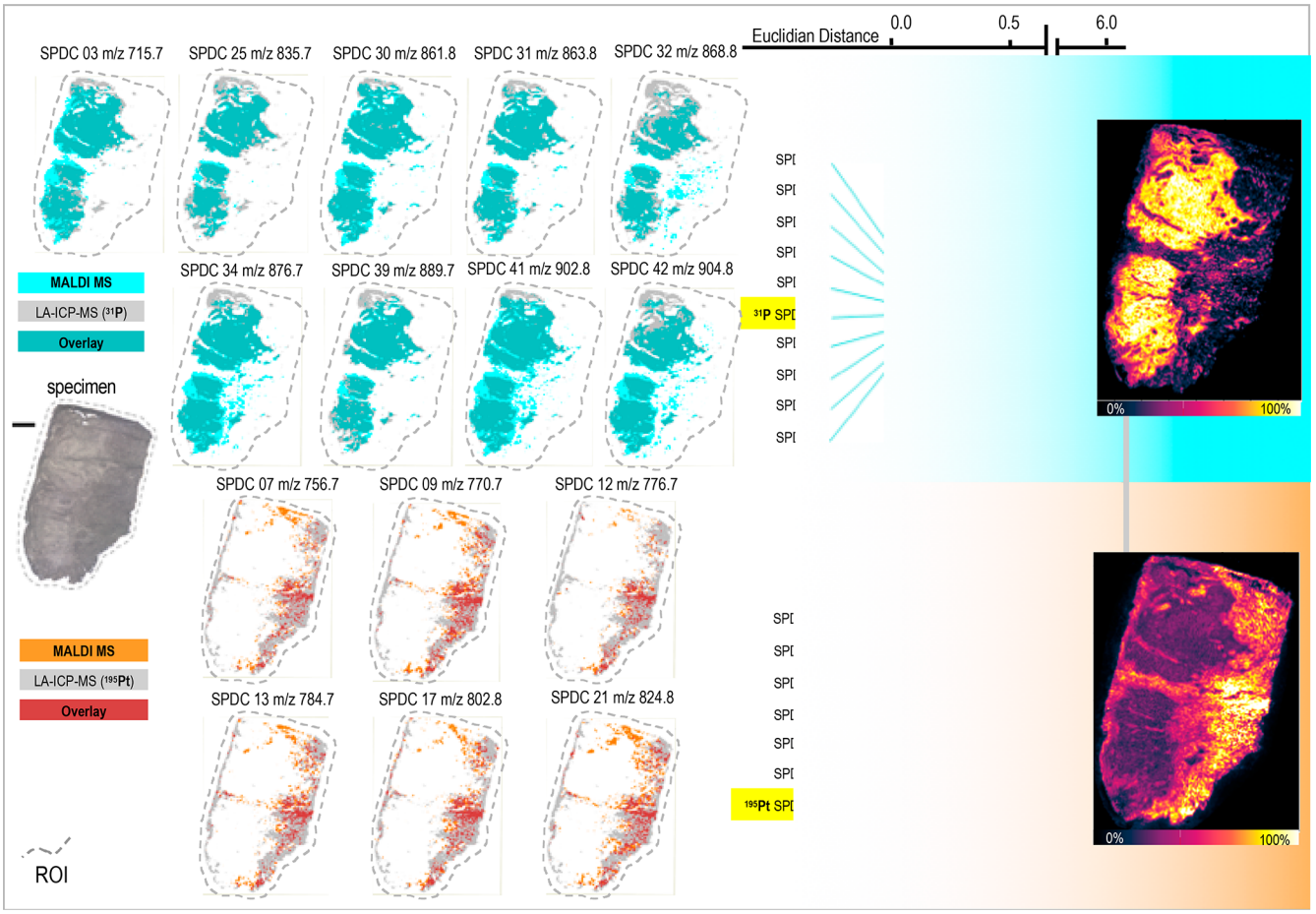

Figure 4. Cluster analysis of the loadings of the first two principal components revealing two subclusters (right side). Elemental and molecular ion overlays are shown representing an intensity threshold level of 50% (cyan, phosphorus related m/z; orange, platinum related m/z; gray, ^{195}Pt and ^{31}P). The scale bar is 1 mm.

desorbed and ionized from each measured spot but numerous components of low abundance in the given ion selection window (±2 Da) increase the number of background signals, which ultimately results in MS/MS spectra exhibiting mixed structural information. A workaround is high-resolution mass spectrometry (HRMS) or tissue lysis in combination with LC-MS/MS to isolate and identify analytes. However, HRMS was not available and LC-MS is an inadequate approach if lateral distribution information is needed. Therefore, MALDI MS/MS was performed directly from tissue for selected mass values with high abundances, giving insight into the structural nature of the detected lipids. Examples are shown in Figure S3, where MS/MS spectra of m/z 861.8 and 863.8 (negative ion mode) exhibit fragments corresponding to phosphatidylinositols (PIs). An exemplary MS/MS spectrum of m/z 1520.3 in Figure S4 proves the presence of lipid dimers in the higher mass range (m/z > 1000).

Multisensor Multimodal Imaging (MSMMI) of MPM Tissue. Imaging by LA-ICPMS and MALDI MS delivered valuable insights into the morphological nature of the present tumor sample and the respective platinum interaction. To further increase information depth, an integrated data evaluation approach was prospected. For this task, the very same tissue sample already analyzed by MALDI MSI was also measured using LA-ICPMS.

As some tissue material is assumed to be ablated during the MALDI MS analysis, quantification of the platinum content in this sample seemed to be doubtful. Additionally, the washing step of the sample prior to MALDI MSI analysis might lead to a wash-out of metals which are only loosely bound to the biological matrix. Such an effect has already been reported in an earlier study and was observed especially for alkaline metals.[19]

The validity of the quantification approach used for platinum in tissue thin-cuts has already been demonstrated earlier by a comparison of values obtained by this approach with bulk platinum concentrations determined by liquid ICPMS after acid digestion of samples.[33]

To obtain an estimate for the validity of the quantification, the average platinum content found in this sample was compared to the one found in the sample which had only been analyzed using LA-ICPMS.

For this, all pixels from the respective sample area were averaged to obtain a mean value for the platinum concentration. While the MPM section analyzed by LA-ICPMS alone only yielded 1.75 μg of platinum/g of tissue, the MPM section analyzed by MALDI MS prior to LA-ICPMS showed an average of 1.91 μg/g. Given the fact that consecutive sections potentially differ in cell content, tumor morphology, and section thickness due to cryo-sectioning, the relative deviation of less than 10% between the two averages can be considered to be negligible. Thus, it can be stated that MALDI MSI analysis does not ablate significant amounts of platinum from the tissue sample, allowing reliable quantitative

DOI: 10.1021/acs.analchem.8b00816
Anal. Chem. 2018, 90, 8831−8837

distribution maps of elements to be obtained even from a sample already analyzed by MALDI MSI. Furthermore, the results indicate that the washing step prior to MALDI-MS analysis does not lead to a significant decrease of the average platinum concentration in the tissue.

Data Evaluation of Multimodal Distribution Images. As the data structure of different analytic methods might be considerably different from each other, it is not obvious that multivariate methods commonly used in image analysis yield reliable and comparable results when applied to multisensor multimodal images. We therefore applied three different methods to compare with each other: PCA, *k*-means clustering, and random forest based classification.

In total, 94 SPDCs have been created on the basis of the MSMMI data set comprising LA-ICPMS data and MALDI MS data from both polarities. Of these, RDF-based classification exhibited 59 m/z values from MALDI MSI, showing a correspondence to either the phosphorus or the platinum distribution pattern within the tissue. The list of SPDCs with their spectrometric background information is given in Figure S5 along with their ion distributions within the MPM tissue section (Figure S6). The list comprises 61 SPDCs, 2 of elemental origin and 59 of molecular origin.

Of the 59 classified m/z values derived from MALDI MSI, 30 corresponded to the phosphorus distribution pattern (all detected in the negative ion mode) and 29 corresponded to the platinum distribution pattern (22 detected in the negative mode and 7 in the positive ion mode). It has to be pointed out here that, in order to not bias the information content of the data set by duplication of information, signals of lipid dimers were excluded from analysis.

To verify the RDF-based classification approach, further chemometric analysis was applied to the MSMMI data set. Results of the PCA are shown in Figure S7. The plotted loadings of PCs 1 and 2 clearly distinguish the analyte distributions related to phosphorus and platinum (encircled in cyan and orange, respectively).

After defining the most significant contributors to the variance of the combined data set, hierarchical cluster analysis (HCA) of the loadings of the PCA could be performed. In Figure 4, the two resulting subclusters of the HCA show a distinction between the viable tumor region (phosphorus related, cyan subcluster) and the assumingly recovered tissue (platinum related, orange subcluster).

Thus, HCA was able to confirm the correlation of analytes detected by MALDI MSI with the elemental distributions of phosphorus and platinum. In Figure 4, those m/z values directly clustering with the two elements are shown as overlays with the respective elemental distribution of phosphorus and platinum. Complete information is given in Figure S8 of the Supporting Information.

When performing *k*-means clustering, a number of clusters has to be assumed prior to the calculations. Here, four clusters were selected as the target number. This number is based on visual examination of the score-plots shown in Figure S9, which suggests the occurrence of four major clusters. Results of *k*-means clustering are shown in Figure S10. Accordingly, results from the *k*-means cluster analysis could be combined with the results from PCA and HCA of the PCA, as shown in Figure 5. Clusters 2 and 4 from the *k*-means clustering are shown in Figure 5c, exhibiting 8528 and 3856 pixels, respectively. They clearly resemble the elemental distributions of phosphorus and platinum, as shown in Figure 5a in cyan and orange, respectively. Further comparability is given with the subcluster of the HCA of the PCA loadings (Figure 5b). *k*-Means clustering also allowed extracting component spectra of the viable tumor areas and the assumingly recovered tissue. The corresponding results are shown in Figure 5 (lower part). Notably, areas with viable tumor tissue (cyan) show higher abundances of phospholipid dimers in positive ion mode (Figure 5f), a finding that correlates well with the higher phosphorus signals detected in the same areas (Figure 5d). This finding supports the assumption that the higher amounts of phosphorus detected in the viable tumor areas indeed correspond to the presence of phospholipids.

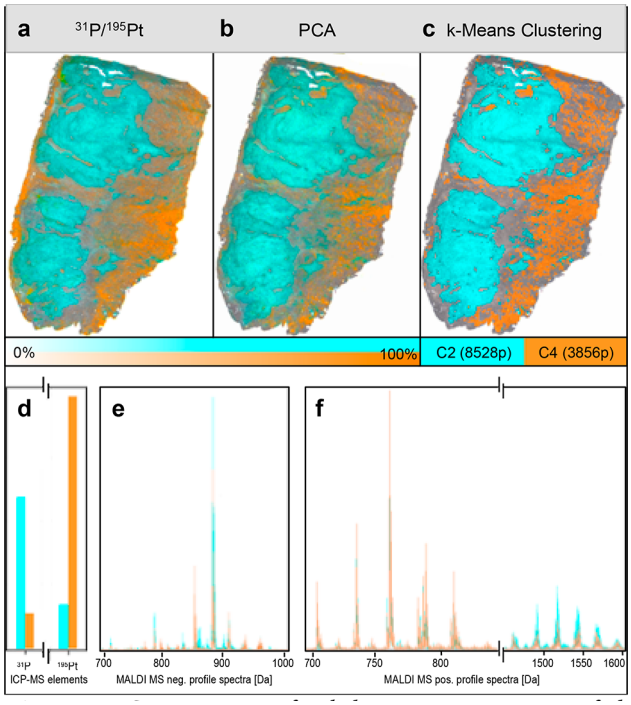

Figure 5. Superposition of a light-microscopic image of the MPM sample and elemental distribution of $^{31}P/^{195}Pt$ (a), results from the HCA of the PCA loadings (b), and clusters 2 and 4 from *k*-means clustering (c); extracted cluster spectra from *k*-means clustering of the MSMMI data set (d–f).

In contrast, the negative ion spectra (Figure 5e) do not exhibit any obvious structural differences between the two clusters.

It is assumed that high phospholipid abundance in the viable tumor areas corresponds to the higher metabolic activity in these regions. However, we present a proof-of-principle study and biologically valid hypotheses can only be proposed after further studies.

CONCLUSION AND OUTLOOK

Results from this study show that the combination of multiple analysis techniques is able to enhance the information depth obtained from one sample to a great extent. Especially the combination of elemental and molecular analysis techniques offers advantages as the results are truly complementary, more accurate because biological variations from different tissue sections are eliminated and the obtained information is not overlapping.

We showed for the first time that it is possible to use one tissue section for both negative and positive mode MALDI MS

DOI: 10.1021/acs.analchem.8b00816
Anal. Chem. 2018, 90, 8831–8837

and subsequently measure quantitatively elemental distributions by LA-ICPMS. This approach allowed maximum correlation of data sets in contrast to the usually performed analysis of consecutive thin-cuts.

Furthermore, we present for the first time that RDF-based calculations identify numerous lipid distributions in the MALDI data set correlating either to the phosphorus or the platinum distribution pattern. The statistical validity of the RDF derived mass list was verified by multivariate statistics.

In future studies, we aim at the application of our innovative methodology in medical studies, providing larger sample stocks to obtain biologically relevant information. Using the presented approach, it will be possible to correlate elemental features not only with lipids but also with any other type of analyte, i.e., proteins, peptides, metabolites, and drugs, leading to an enhanced understanding of biological processes such as tumor genesis or the mechanism of action of antitumor drugs.

■ ASSOCIATED CONTENT

Supporting Information

The Supporting Information is available free of charge on the ACS Publications website at DOI: 10.1021/acs.analchem.8b00816.

Exemplary MALDI MSI profile spectra, exemplary tandem MALDI mass spectra, list of spectral descriptors, LA ICPMS single ion images and MALDI MSI images, PCA of 61 SPDCs, HCA on the loadings of the PCA (61 SPDCs), PCA (61 SPDCs), and *k*-means clustering (61 SPDCs) (PDF)

■ AUTHOR INFORMATION

Corresponding Author

*Phone: +43-1-58801-15162. Fax: +43-1-58801-915162. E-mail: martina.marchetti-deschmann@tuwien.ac.at.

ORCID

Andreas Limbeck: 0000-0001-5042-2445

Martina Marchetti-Deschmann: 0000-0002-8060-7851

Author Contributions

M.H. and M.B. contributed equally. All authors have given approval to the final version of the manuscript.

Notes

The authors declare no competing financial interest.

■ ACKNOWLEDGMENTS

The authors acknowledge COST Action 1104 and the PhD program MEIBio (supported by TU Wien) for scientific exchange, personnel funding, and valuable discussions. The authors further acknowledge Balazs Hegedus (University of Duisburg-Essen) for providing MPM sections and highly appreciate the support of Prof. Günter Allmaier (TU Wien) for granting access to instrumentation.

■ REFERENCES

(1) Van de Plas, R.; Yang, J.; Spraggins, J.; Caprioli, R. M. *Nat. Methods* **2015**, *12*, 366.

(2) Mascini, N. E.; Cheng, M.; Jiang, L.; Rizwan, A.; Podmore, H.; Bhandari, D. R.; Rompp, A.; Glunde, K.; Heeren, R. M. *Anal. Chem.* **2016**, *88*, 3107−3114.

(3) Aoyagi, S.; Abe, K.; Yamagishi, T.; Iwai, H.; Yamaguchi, S.; Sunohara, T. *Anal. Bioanal. Chem.* **2017**, *409*, 6387−6396.

(4) Vollnhals, F.; Audinot, J. N.; Wirtz, T.; Mercier-Bonin, M.; Fourquaux, I.; Schroeppel, B.; Kraushaar, U.; Lev-Ram, V.; Ellisman, M. H.; Eswara, S. *Anal. Chem.* **2017**, *89*, 10702−10710.

(5) Marty, F.; Rago, G.; Smith, D. F.; Gao, X.; Eijkel, G. B.; MacAleese, L.; Bonn, M.; Brunner, E.; Basler, K.; Heeren, R. M. A. *Anal. Chem.* **2017**, *89*, 9664−9670.

(6) Lasch, P.; Noda, I. *Anal. Chem.* **2017**, *89*, 5008−5016.

(7) Desbenoit, N.; Walch, A.; Spengler, B.; Brunelle, A.; Rompp, A. *Rapid Commun. Mass Spectrom.* **2018**, *32*, 159−166.

(8) Lanni, E. J.; Dunham, S. J.; Nemes, P.; Rubakhin, S. S.; Sweedler, J. V. *J. Am. Soc. Mass Spectrom.* **2014**, *25*, 1897−1907.

(9) Eberlin, L. S.; Liu, X.; Ferreira, C. R.; Santagata, S.; Agar, N. Y. R.; Cooks, R. G. *Anal. Chem.* **2011**, *83*, 8366−8371.

(10) Bianga, J.; Bouslimani, A.; Bec, N.; Quenet, F.; Mounicou, S.; Szpunar, J.; Bouyssiere, B.; Lobinski, R.; Larroque, C. *Metallomics* **2014**, *6*, 1382−1386.

(11) Günther, D.; Hattendorf, B. *TrAC, Trends Anal. Chem.* **2005**, *24*, 255−265.

(12) Russo, R. E.; Mao, X.; Liu, H.; Gonzalez, J.; Mao, S. S. *Talanta* **2002**, *57*, 425−451.

(13) Becker, J. S. *Spectrochim. Acta, Part B* **2002**, *57*, 1805−1820.

(14) Orellana, F. A.; Gálvez, C. G.; Orellana, F. A.; Gálvez, C. G.; Roldán, M. T.; García-Ruiz, C.; Roldán, M. T.; García-Ruiz, C. *TrAC, Trends Anal. Chem.* **2013**, *42*, 1−34.

(15) Resano, M.; Garcia-Ruiz, E.; Vanhaecke, F. *Mass Spectrom. Rev.* **2010**, *29*, 55−78.

(16) Becker, J. S.; Zoriy, M.; Matusch, A.; Wu, B.; Salber, D.; Palm, C.; Becker, J. S. *Mass Spectrom. Rev.* **2009**, *29*, 156−175.

(17) Drescher, D.; Giesen, C.; Traub, H.; Panne, U.; Kneipp, J.; Jakubowski, N. *Anal. Chem.* **2012**, *84*, 9684−9688.

(18) Dreisewerd, K. *Anal. Bioanal. Chem.* **2014**, *406*, 2261−2278.

(19) Limbeck, A.; Galler, P.; Bonta, M.; Bauer, G.; Nischkauer, W.; Vanhaecke, F. *Anal. Bioanal. Chem.* **2015**, *407*, 6593−6617.

(20) Spengler, B. *Anal. Chem.* **2015**, *87*, 64−82.

(21) Bouschen, W.; Schulz, O.; Eikel, D.; Spengler, B. *Rapid Commun. Mass Spectrom.* **2010**, *24*, 355−364.

(22) Hankin, J. A.; Barkley, R. M.; Murphy, R. C. *J. Am. Soc. Mass Spectrom.* **2007**, *18*, 1646−1652.

(23) Yang, J.; Caprioli, R. M. *Anal. Chem.* **2011**, *83*, 5728−5734.

(24) Gonzalez de Vega, R.; Sanchez, M. L. F.; Eiro, N.; Vizoso, F. J.; Sperling, M.; Karst, U.; Medel, A. S. *Anal. Bioanal. Chem.* **2018**, *410*, 913.

(25) Niehoff, A.-C.; Schulz, J.; Soltwisch, J.; Meyer, S.; Kettling, H.; Sperling, M.; Jeibmann, A.; Dreisewerd, K.; Francesconi, K. A.; Schwerdtle, T.; Karst, U. *Anal. Chem.* **2016**, *88*, 5258−5263.

(26) Ellis, S. R.; Solwitsch, J.; Paine, M. R. L.; Dreisewerd, K.; Heeren, R. M. A. *Chem. Commun.* **2017**, *53*, 7246−7249.

(27) Ellis, S. R.; Cappell, J.; Potocnik, N. O.; Balluff, B.; Hamaide, J.; Van der Linden, A.; Heeren, R. M. *Analyst* **2016**, *141*, 3832−3841.

(28) Thomas, A.; Charbonneau, J. L.; Fournaise, E.; Chaurand, P. *Anal. Chem.* **2012**, *84*, 2048−2054.

(29) Deininger, S. O.; Becker, M.; Suckau, D. *Methods Mol. Biol.* **2010**, *656*, 385−403.

(30) Angel, P. M.; Spraggins, J. M.; Baldwin, H. S.; Caprioli, R. *Anal. Chem.* **2012**, *84*, 1557−1564.

(31) Holzlechner, M.; Strasser, K.; Zareva, E.; Steinhäuser, L.; Birnleitner, H.; Beer, A.; Bergmann, M.; Oehler, R.; Marchetti-Deschmann, M. *J. Proteome Res.* **2017**, *16*, 65−76.

(32) Bonta, M.; Lohninger, H.; Marchetti-Deschmann, M.; Limbeck, A. *Analyst* **2014**, *139*, 1521−1531.

(33) Bonta, M.; Lohninger, H.; Laszlo, V.; Hegedus, B.; Limbeck, A. *J. Anal. At. Spectrom.* **2014**, *29*, 2159−2167.

(34) Lohninger, H.; Ofner, J. *Spectrosc. Eur.* **2014**, *26*, 6−10.

(35) Lohninger, H.; Varmuza, K. *Anal. Chem.* **1987**, *59*, 236−244.

(36) Breiman, L. *Machine Learning* **2001**, *45*, 5−32.

(37) Ofner, J.; Kamilli, K. A.; Eitenberger, E.; Friedbacher, G.; Lendl, B.; Held, A.; Lohninger, H. *Anal. Chem.* **2015**, *87*, 9413−9420.

DOI: 10.1021/acs.analchem.8b00816
Anal. Chem. 2018, 90, 8831−8837